N O T I C E

THIS DOCUMENT HAS BEEN REPRODUCED FROM MICROFICHE. ALTHOUGH IT IS RECOGNIZED THAT CERTAIN PORTIONS ARE ILLEGIBLE, IT IS BEING RELEASED IN THE INTEREST OF MAKING AVAILABLE AS MUCH INFORMATION AS POSSIBLE

A Report

entitled

ANALYTICAL STUDY OF TWIN-JET SHIELDING
SECOND ANNUAL PROGRESS REPORT

NASA Grant No. NAG 1-11

Submitted by the

TEXAS A & M RESEARCH FOUNDATION

to

National Aeronautics and Space Administration
Langley Research Center

Prepared by

Dr. Carl H. Gerhold

of the

Department of Mechanical Engineering
Texas A & M University
College Station, Texas 77843

RECEIVED
NASA STI FACILITY
ACCESS DEPT.

January, 1982

(NASA-CR-165102) ANALYTICAL STUDY OF TWIN-JET SHIELDING Annual Progress Report (Texas A&M Univ.) 39 p HC A03/MF A01 CSCL 20A

N82-16801

Unclas
G3/71 05405

Table of Contents | Page

List of Figures iii

I. INTRODUCTION 1

II. COMPARISON TO POINT NOISE SOURCE SHIELDING EXPERIMENT 3

1. Isothermal Subsonic Jet 4

2. Simulated Hot, Subsonic Jet 6

3. Shielding Jet Widening Algorithm 7

III. DEVELOPMENT OF JET NOISE SOURCE MODEL 9

1. Description of the Jet Noise Model 10

2. Basic Directivity Model 11

3. Spectral Amplitude Functions 11

IV. JET SHIELDING USING MODIFIED SOURCE MODEL 16

1. Jet Noise Spectral Patterns 16

2. Spectrum of Polar Directivity 17

V. SUMMARY 18

Figures 19

REFERENCES 36

List of Figures

Page

1. Schematic Representation of Point Noise Source Shielding Model

2. Azimuthal directivity, Air Jet, $m = .53$, $k_o a = .56$

3. Aximuthal directivity, Air Jet, $m = .53$, $k_o a = 1.60$

4. Polar Directivity, Air Jet, $m = .53$, $\alpha = 180^o$

5. Polar Directivity, Air Jet, $m = .53$, $\alpha = 180^o$

6. Azimuthal Directivity Function Model with Shielding Jet Widening - $k_o a = .56$

7. Azimuthal Directivity Function - Model with Shielding Jet Widening - $k_o a = 1.60$

8. Twin Jet Shielding Comparison with Point Noise Source - Heated Jet, $\alpha = 180^o$

9. Typical Polar Directivity Plot of Unheated, Supersonic Jet Noise

10. Relative Spectral Distribution of Isothermal Jet Noise at $\psi_n = 90^o$

11. Relative Spectral Distribution of Isothermal Jet Noise at $\psi_n = 30^o$

12. Polar Directivity of Unheated, Supersonic Jet Noise at St = 0.12

13. Polar Directivity of Unheated, Supersonic Jet Noise at St = 0.25

14. Polar Directivity of Unheated, Supersonic Jet Noise at St = 0.50

15. Spectral Distribution of Twin, Unheated Jets, Comparing Unshielded ($\alpha = 90^o$) to Shielded ($\alpha = 180^o$) Spectra. $\psi_n = 60^o$

16. Spectral Distribution of Twin, Heated Jets, Comparing Unshielded ($\alpha = 90^o$) to Shielded ($\alpha = 180^o$) Spectra. $\psi_n = 30^o$

17. Twin Jet Shielding Comparison with Modified Point Noise Source - Heated Jet, $\alpha = 180^o$

Analytical Study of Twin-Jet Shielding

I. INTRODUCTION

This report summarizes progress in the refinement and evaluation of the analytical jet shielding model. Development of the basic model is shown in the previous annual progress report (1). The model consists of a point noise source impinging on a cylinder of heated flow in which the temperature and velocity are uniform across the cross-section of the jet. The shielding jet is infinite in extent along the jet axis and the radius of the jet is constant.

The analytical model is compared to experimental data for a point noise source impinging on an ambient temperature, subsonic jet; and on a subsonic simulated hot jet using helium as the flow medium (2). The results of these comparison are discussed in the present report. It is found that the model estimates the same trends as the experiment. Agreement is best in the shadow zone at receiver locations directly opposite jet from the source. As the receiver moves downstream from the source, the model estimates less shielding than experiment indicates. This is felt to be due to the fact that the actual shielding jet widens downstream of the jet nozzle due to mixing with the quiescent air surrounding the jet. Preliminary results using a jet widening algorithm in the analytical model indicate that the decreased diffraction around the widening jet results in greater downstream shielding, in agreement with experimental trends.

Previous comparison of the analytical model to twin jet shielding experiments had indicated discrepancies (1). It was felt that the differences should be resolved by refinement of the jet noise source model. The modification of the source term is intended to represent the directional nature of the jet noise radiation pattern. This report summarizes the development of the jet noise source model. The source strength term is redefined with a directivity imposed

imposed. The modified source term incorporates not only the spatial variation of the jet noise, but also the frequency spectrum. The modified source model is found to compare favorably to jet noise measurements of a cold supersonic jet and an ambient temperature jet of Mach number 0.5 to 1.95. The modified noise source term is found to improve the comparison between the model and the twin-jet shielding experiment at receiver locations in the near downstream region. As with the point source comparison, the model estimates less shielding further downstream. This discrepancy is felt to result from the added barrier effect due to jet widening in the real shielding jet.

II. COMPARISON TO POINT NOISE SOURCE SHIELDING EXPERIMENT

The derivation of the total far field sound pressure has been shown in the previous annual report (1). The normalized sound pressure level at a receiver in the acoustic far field is expressed as a directivity function, ΔSPL,

$$\Delta SPL = 10 \log_{10} \left| \frac{P_T}{P_{in}} \right|^2 (dB) \tag{1}$$

where:

P_T = Total, incident plus scattered, sound pressure

P_{in} = Incident sound pressure at the location

$\Delta SPL > 0$ indicates sound amplification

$\Delta SPL < 0$ indicates sound reduction.

Measurements of the sound pressure level from a point source near a jet have been made by Yu and Fratello at NASA-Langley Research Center (2). For the purposes of testing the analytical model, comparison of the measured shielding to the shielding estimated by the model are made. Test cases include an isothermal Mach number 0.53 air jet and a simulated hot air Mach 0.18 jet using helium as the flow medium. In the experiments, the noise source is located 4 jet diameters downstream of the shielding jet nozzle exit, and at a lateral spacing of 2.5 jet diameters.

The coordinate system is centered on the sound source, and is illustrated in Figure 1. In the nomenclature adopted for the comparison, $\psi_n = 0^o$ on the z-axis of the source, parallel to the shielding jet. The angle α is 0° when the receiver is on the source side of the jet; and 180° when the receiver is directly opposite the jet from the source.

1. Isothermal Subsonic Jet

Figures 2 and 3 show the modification of the directivity function by the shielding jet in azimuthal planes downstream of the source. The curves in figure 2 are for the normalized frequency parameter, $k_o a = 0.56$, where:

k_o = wave number = $2\pi f/c_o$

a = shielding jet radius.

Figure 3 is for $k_o a = 1.6$

At low frequency, Figure 2, the shielding effect is small. At the near downstream locations, $\psi_n = 75^o$, incident sound is transmitted through the jet, and back scattering is negligible. As the receiver moves downstream from the source, the shadow zone, in which ΔSPL is less than zero, becomes more well defined. The zone becomes wider and the maximum attenuation increases as the jet axis is approached ($\psi_n \rightarrow 0^o$). The sound is scattered into a lobe immediately adjacent to the shadow zone.

At higher frequency, Figure 3, the broadening of the shadow zone is less, but the maximum attention is greater. The lobe of amplification adjacent to the shadow zone shifts toward the source side of the shielding jet and becomes wider as the jet axis is approached. A smaller and less intense zone of sound reduction is seen adjacent to the lobe of amplification. This zone shifts toward the source side of the jet as the axis is approached, and disappears at $15^o < \psi_n < 30^o$.

The trends exhibited by the model compare favorably with experiment for both low and high frequency. The measured data show lobe formations similar to those estimated. The model under estimates the maximum sound reduction in the shadow zone at receiver locations near the jet axis ($\psi_n < 30^o$). The discrepency increases with frequency.

The directivity function is evaluated on the side of the jet directly opposite the source, for $\psi_n < 90^\circ$ (downstream of the source) and for $\psi_n > 90^\circ$ (upstream of the source). The plot is shown in Figure 4.

Sound is scattered into the region upstream of the source, $\psi_n > 90^\circ$, and the magnitude of the amplification increases with frequency. As the receiver moves downstream from the source, $\psi_n < 90^\circ$, sound is attenuated. The rate of sound reduction is at first gradual, and then increases at the angle, $\psi_n \simeq 50^\circ$. For angles within the range:

$$90^\circ > \psi_n > 50^\circ$$

transmission of noise through the jet is dominant. Within this range, low frequency sound is transmitted through the jet more readily than higher frequency sound.

The transmission cut-off angle is the angle greater than which, theoretically, all sound is transmitted. At angles of incidence less than the cut-off, no sound is transmitted through the jet (3). The expression for the transmission cut-off angle reported in reference 3:

$$\psi_{nct} = \cos^{-1} \left[\frac{c_o/c_j}{1 + M} \right] \tag{2}$$

where:

c_o = sound speed at the ambient temperature

c_j = sound speed at jet temperature

M = jet Mach number, V/c_j

was also found by investigation of the terms in the expression for the far field total sound pressure in the previous annual report (1). For the parameters of the jet under investigation:

$$\psi_{nct} = 49^\circ$$

It is expected, and shown in Figure 4, that transmission through the jet dominates at angles in the range $49^\circ < \psi_n < 90^\circ$. While sound is still transmitted

at angles, $\psi_n < 49^o$, the influence of sound transmission decreases rapidly as sound is refracted downstream in the jet. The decrease in sound transmission is frequency dependent as shown in Figure 4. The transmitted sound falls off more rapidly as frequency increases.

As the jet axis is approached ($\psi_n \rightarrow 0^o$), and the transmitted sound contribution diminishes, sound diffracted around the jet becomes dominant. This diffracted sound imposes a theoretical limit on the shielding of approximately 6 dB.

The analytical results show agreement in form with the experimental results. The model underestimates the magnitude of sound scattering upstream of the source. The model follows closely the trend of the measured data in the transmission dominant zone. As the jet axis is approached, the measured sound level continues to decrease; while the model approaches a sound reduction limit. This indicates that diffraction is a less dominant mechanism in shielding by the real jet.

2. Simulated Hot, Subsonic Jet

The purpose for development of the model is to estimate the shielding for heated jets. For this reason, the model is compared to a simulated hot jet using helium as the flow medium. In this jet, the density ratio, $\rho_j/\rho_o = 1/7$ and the sound speed ratio, $c_j/c_o = 3.0$. The jet mach number, $V/c_j = 0.18$.

Figure 5 shows the directivity function on the side of the jet opposite the source at the normalized frequencies, $k_o a$, of 0.56 and 1.6. The curves are similar to the unheated jet, Figure 4. The expected transmission zone cut-off angle:

$$\psi_{nct} = 74^o$$

is well defined at low frequency, $k_o a = 0.56$. Unlike the unheated jet, the directivity function is less than zero upstream of the source. This may indicate that the density difference between the ambient air and the jet stream causes

scattering toward the source side of the shielding jet.

The model estimates the trends of the experimental data for upstream locations. The sound reduction upstream of the noise source is shown. The model follows the trend of the experimental data in the near downstream region. As with the unheated jet, the model shows greater influence of diffraction further downstream than does the experiment.

3. Shielding Jet Widening Algorithm

The model estimates the trend of shielding, not only on the side of the jet opposite the source, but also in the azimuthal planes downstream of a source impinging on the unheated jet. The model agrees in form with the shielding by the simulated hot jet. In the region near the jet axis, the trend of the model diverges from experiment. The models for both the unheated jet and the simulated hot jet show greater dependence on diffraction of sound around the jet. Thus, the noise source is seeing a more effective sound barrier than the model estimates.

The increase in barrier dimension is felt to be accommodated by the widening of the jet. In the present analysis, the shielding jet is modelled as an infinite cylinder of constant cross-section, where the actual jet widens downstream. As the jet widens, it becomes more effective as a sound barrier. Thus, less sound is diffracted into the shadow zone on the side of the jet opposite the source. From barrier theory, the scattering effect is more pronounced as the frequency increases. Thus, the jet widening alters the diffracted noise pattern more at high frequency than at low frequency.

In order to test the validity of the assumption that jet widening resolves the discrepancies noted, a jet widening algorithm has been included in the model. Figures 6 and 7 show the effect of the shielding jet widening downstream of the nozzle, for the isothermal jet. In these figures, the jet spreads

at an included angle of 24°. The increase in jet cross section is accompanied by a decrease in velocity in the jet. In the model, the slug flow approximation is retained; but the mean velocity is assumed to decrease linearly with downstream distance.

The jet widening does not affect the plots of ΔSPL for $\psi_n > 60^{\circ}$. However, in this zone the difference between the model and experiment is not large. For $\psi_n < 60^{\circ}$, jet widening has a more pronounced effect. Since the spreading of the jet alters the sound diffraction pattern, the effect is more pronounced as frequency increases. At low frequencies, $k_o a = .56$, the sound is scattered into a lobe of amplification adjacent to the shadow zone. (Figure 6). As ψ_n increases, this lobe of amplification shifts toward the source side of the jet and broadens. At locations near the source axis, the lobe of amplification disappears altogether.

At higher frequency, $k_o a = 1.6$, the lobe of amplification is preceded by a lobe of sound reduction, as shown in Figure 7. As ψ_n decreases, the curve is shifted toward the source side; with the lobe of sound reduction disappearing between $\psi_n = 30^{\circ}$ and $\psi_n = 15^{\circ}$, and then the lobe of amplifiation disappearing at $\psi_n < 15^{\circ}$.

The experimental results show a similar trend. However, the shifting of the curves toward the source side is more gradual than the model estimates.

The jet widening algorithm chosen has over-corrected the model. However, results indicate that inclusion of spreading in the shielding jet model can resolve, in large part, the discrepancies between the model and experiment. Continuing research will be directed toward refinement of the widening algorithm.

III. DEVELOPMENT OF JET NOISE SOURCE MODEL

The analytical model was compared to experimental twin-jet results in the previous annual report (1). The comparison is redrawn in Figure 8. In the figure, the abscissa is normalized frequency, $k_o a$. The ordinate is the normalized sound pressure, expressed as ΔSPL in dB., as employed in the previous section of this report. The operating conditions reported by Kantola (4) are as follows:

$T_j = 1238\ ^oR$

$V_j = 1519$ Fps

$S/D = 2.67$

$\alpha = 180^o$

The receiver is in the far field in the shadow zone of the shielding jet. That is, the shielding jet is between the source jet and the receiver. Two receiver locations are investigated. The first is in the near down-stream region of the jet exit ($\psi_n = 60^o$) and the second is closer to the jet axis ($\psi_n = 30^o$). The experimental data has been corrected to eliminate the noise emitted by the shielding jet.

From Figure 8, the model appears to follow the trend of experiment at locations close to the jet axis ($\psi_n = 30^o$). At low frequency, the shielding increases rapidly for $k_o a$ approaching 1.0. As the frequency increases from $k_o a = 1.0$ to $k_o a = 10.0$, the rate of noise reduction decreases. The model and experiment typically agree to within ± 2.0 dB. At receiver locations in the near downstream region, $\psi_n = 60^o$; the trends shown by the model and by experiment diverge. The experimental data show a more gradual increase in noise reduction with frequency than do the model results. The discrepancies between model and experiment were felt to be due to the difference between the noise radiation patterns of point noise source and the actual heated jet (1). For

this reason, a more realistic representation of the jet noise emission has been developed by Kim (5).

1. Description of the Jet Noise Model

The source term in the wave equation has the form:

$$\frac{Q_o}{r} e^{-i\omega t} \delta(r-r_o)\delta(\theta)\delta(z)$$

For a point noise source, the source strength, Q_o, is constant. The jet noise model is developed by a formulation for the source strength in which the directivity is imposed. Figure 9 shows a typical plot of polar directivity of the jet noise from measurements by Yu and Dosanjh (6). In the figure, the sound pressure at the polar coordinate is normalized by the sound pressure at the peak.

As shown in figure 9, the far field sound pressure level contours are characterized by a peak, located between 25° and 30° from the jet axis, and diminishing values on either side of the peak. Physically, this states that, due to the convection effect, the sound waves are crowded in the downstream direction and more widely spaced in the upstream direction. This enhances the intensity in directions making an acute angle with the flow. At the same time, sound rays are refracted by the mean flow, weakening the sound along the core of the jet. Thus, the sound pressure near the jet axis is dominated by this refractive bending of the sound waves.

The general form of the noise source model selected for the present study is suggested by Ribner's analysis (7). The far field mean square sound pressure is made up of a basic directivity function, which defines the spectral shape, and a convection factor. The convection factor is the Lighthill convection factor modified to show the amplification downstream due to the source convection. The source amplitude, Q, based on Ribner's model is:

$$Q = \frac{U_j^4 D}{c_o^2} DI(CS,\psi_n)^{\frac{1}{2}} C^{-5/2} \tag{3}$$

where:

$\frac{U_j^4 D}{c_o^2}$ = amplitude based on Lighthill's U_i^8 velocity dependence

DI = the basic directivity function

CS = modified Strouhal number = CfD/U_j

C = the basic convection factor

= $[(1-M_c \cos \psi_n)^2 + \alpha^2 M_c^2]^{\frac{1}{2}}$

m_c = effective average source convection speed/c_o

= $1.5U_j/c_o$

α = non-dimensional parameter

2. Basic Directivity Model

Ribner suggests that the basic directivity function is composed of two spectral components. One component is a function of self-noise due to turbulence alone; while the other is a shear noise term arising from a cross coupling of the turbulence with the mean flow shear. The basic form of the directivity function has been modified by Kim in order to improve the fit to experimental data, where:

$$DI(\psi_n,CS) = \left[A(CS)\left(\frac{1+3\sin^2\psi_n}{4}\right) + B(CS)(8\sin^2{}_n\cos^6\psi_n)\right]^{\frac{1}{2}} \tag{4}$$

where:

A = spectral amplitude due to self-noise

B = spectral amplitude due to shear noise.

3. Spectral Amplitude Functions

The choice of A and B for the best fit with the experimental data has been studied by Nosseir and Ribner (8). It is obserbed that the values of A

and B fall on two reasonably smooth curves: the self-noise spectral peak lies roughly an octave above the shear noise spectral peak. This is based on the argument that the spectral component, $e^{i\omega t}$, in shear noise appears as $e^{2i\omega t}$ in the self noise due to squaring of the turbulent velocity component. Thus,

$$B(CS) = 2A(2CS)$$

Thus the two amplitude functions have the same shape. The shear noise spectrum is shifted by an octave and its amplitude is twice that of the self noise. Ribner (7) assumes that a semi-empirical spectral shape function with the correct assymptotic behavior has the form:

$$\frac{\nu^2}{(1+\nu^2)^2}$$

where:

$$\nu = 2\pi\ CS$$

The specific form of the spectral amplitude functions was obtained by comparison to experimental data of Tanna and Dean (9), shown in Figures 10 and 11, for an isothermal jet ($T_j = T_o$). Variations of 1/3 octave spectral shapes at 30° and 90° from the jet axis where the Mach number is varied from 0.5 to 1.95, is investigated. Tanna and Dean observe that at $\psi_n = 90^o$, the spectral shape has a broad peak. In contrast, at $\psi_n = 30^o$, the spectrum shifts toward lower frequency and the peak becomes more marked.

Kim has found the best fit to experimental data to be made using the amplitude functions:

$$A(\nu) = \frac{(\nu/4)^2}{[1 + (\nu/4)^2]^{3/2}} \tag{5a}$$

$$B(\nu) = \frac{2(\nu/2)^2}{[1 + (\nu/2)^2]^{3/2}} \tag{5b}$$

The estimated spectral shapes are shown by the solid lines on figures 10 and 11. In Figure 10 at $\psi_n = 90^o$, the model estimates the trend of the curves to decrease in intensity as flow speed decreases. The agreement between the model and experiment is good at frequencies less than the peak for all flow speeds. The model estimates a greater roll off of sound intensity at high frequency than is measured. At $\psi_n = 30^o$, the polar location at which the overall jet noise is most intense, the estimate shows good agreement with experiment for $U_j/c_o < 1$. For $U_j/c_o > 1$, the model is more sensitive to changes in flow speed than experiment indicates. While the estimated spectra are narrower than those estimated at $\psi_n = 90^o$, they are broader than the measured spectra. Finally, the shift toward higher frequency of the peak noise with increasing flow speed is greater in the model than is measured. The estimate peak occurs at a frequency between 1½ and 2 decades higher than is found experimentally at the higher flow speeds.

Since the peak of the overall jet noise pattern is located at a polar location of approximately 30° from the jet axis, the estimated shiedling is expected to be most sensitive to the source noise spectrum at $\psi_n = 30^o$. From Figure 11, the spectral amplitude function is expected to be most reliable for subsonic jet flows for the isothermal jet.

The formulation of the jet noise source strength, Q, incorporates the directivity pattern, convection effect, velocity dependence and spectral shape function. This semi-emperical term is summarized below:

$$Q = \frac{U_j^4 D}{c_o^2} \left[\frac{(\nu/4)^2}{[1+(\nu/4)^2]^2} \frac{(1+3\sin^2\psi_n)}{4} + \frac{16(\nu/2)^2}{[1+(\nu/2)^2]} (\sin^2\psi_n \cos^6\psi_n) \right]^{1/2} \quad (6)$$

$$\times\ c^{-5/2}$$

The far field noise radiation estimated using the source term above is compared to experimental data of Yu and Dosanjh (6). The jet operating conditions are:

$M_j = 1.5$

$T_j = 365.8\ ^oR$

$T_o = 530.4\ ^oR$

Figures 12, 13 and 14 show the polar directivity of the jet noise. In the figure, the sound pressure is normalized by the sound pressure at the peak location. The data in Figure 12 are measured at a Strouhal number, St = 0.12, where:

$$St = \frac{fD}{U_j}$$

in which:

f = frequency

D = jet diameter

U_j = jet exit velocity

Figure 13 is measured at St = 0.25 and Figure 14 is for St = 0.5.

The figures generally show good agreement with the measured jet noise pattern. The model estimates the location of the peak and the rapid decrease in sound pressure level on either side of the peak. The rate of sound reduction on either side of the peak follows the measured data.

The model for the source strength representative of a jet has been developed. The model consists of a convection factor, which shows the downstream amplification due to source convection; a basic directivity function which defines the spectral shape; and an amplitude based on Lighthill's U_j^8 velocity dependence. The model estimates the polar directivity of a cold, supersonic jet for a range of frequencies corresponding to Strouhal numbers from 0.12 to 0.5. The model estimates the form of the spectral amplitude and the

relative amplitude dependence on velocity of an isothermal jet at subsonic flow. The model for the spectral amplitude is found to deviate from measured data at supersonic flows for the isothermal jet, at a location near the jet noise peak. This is not felt to be due to an error in the form of the spectral function; but rather to the choice of parameters. It is felt that the relationship, $\nu/4$, in the basic amplitude function makes the function over-sensitive to changes in flow speed. A relationship closer to $\nu/2$, as suggested by Ribner, makes the function less sensitive to flow speed change; which is the trend of the experimental data.

The form of the source strength is preferred because of its adaptability to the shielding model originally developed. No change in the basic formation of the model is necessitated. The estimated sound pressure at the receiver is still based on a point noise source. However, with the modified source model, the source strength is a function, not only of the characteristics of the jet, but also of the receiver location.

IV. JET SHIELDING USING MODIFIED SOURCE MODEL

The noise source model with directivity imposed is incorporated into the shielding model, and the estimated shielding compared to Kantola's experimental data (4).

1. Jet Noise Spectral Patterns

Figures 15 and 16 are the spectral shapes at two locations downstream from the jet exit; near downstream, $\psi_n = 60^\circ$ and approaching the jet axis, $\psi_n = 30^\circ$. The purpose for these comparisons is to ensure that the estimated jet noise spectrum corresponds to that measured by Kantola; since the shielding spectrum depends not only on the frequency dependence of the shielding mechanism, but also on the signature of the jet. In the figures, the sound pressure level is shown both at $\alpha = 180^\circ$, when the receiver is opposite the shielding jet from the source; and at $\alpha = 90^\circ$, when the receiver is equidistant from both jets. The influence of the shielding jet on the source jet is expected to be minimum at $\alpha = 90^\circ$. The estimated spectrum at $\psi_n = 60^\circ$ (Figure 15) follows closely the measured spectrum, showing the rise to the peak and the relatively gradual sound level decrease at frequencies beyond the peak.

At $\psi_n = 30^\circ$, Figure 16, the estimates for both the shielded, $\alpha = 180^\circ$ and unshielded, $\alpha = 90^\circ$ spectra are broader than those measured. The peaks of the spectra are estimated to occur at higher frequencies than are indicated by the measured data. These results are consistent with those noted during the comparison to Tanna and Dean's measurements at $\psi_n = 30^\circ$ in a previous section of this report. At that time, it was noted that the discrepancy was felt to arise from the choice of parameters in the spectral amplitude function. Preliminary investigation into the effect of modifying this parametric relationship indicates that both the shielded and unshielded curves are affected similarly. Thus, the difference between the two curves remains the same as shown in Figure 16.

2. Spectrum of Polar Directivity

The difference between the $\alpha = 180^{\circ}$ and $\alpha = 90^{\circ}$ spectra in Figures 15 and 16 gives the relative sound pressure level, ΔSPL. The resulting spectrum eliminates the noise emitted by the shielding jet. This directivity function was plotted in Figure 8 for the constant strength source and is plotted in Figure 17 for the source with directivity imposed.

The estimated shielding using the modified source shows considerable improvement over the estimate with the constant strength point source at $\psi_n = 60^{\circ}$. The estimated curve follows measured data over the entire range of frequencies up to $k_o a = 10.0$. At locations closer to the jet axis, $\psi_n = 30^{\circ}$, the estimated shielding is less than the measured shielding by as much as 4 dB. However, the forms of the estimated and measured shielding curves are similar.

The agreement of the measured and analytical results in the near downstream region; and disagreement as the jet axis is approached is consistent with the comparison to the point source shielding in a previous section. The model shows more diffraction of sound around the shielding jet that is measured. Thus, the difference noted at $\psi_n = 30^{\circ}$, in Figure 17, is felt to be attributable in large part to the jet widening, which will be investigated in the period of continued effort for this project.

V. SUMMARY

The shielding model with a point noise source has been compared to experimental shielding of a point source. The results have shown similarities in trend with differences noted in the far downstream region. It is contended, and verified by preliminary results, that added barrier effect of the widening jet accounts, in large part, for the noted discrepancies. Refinement of the jet widening algorithm in the shielding model is one goal for the continued effort in this project.

A modified noise source formulation has been developed whose purpose it is to represent, more realistically, the spectral and directional emission from a jet. This model has been shown to be applicable to a number of jet applications. The model requires refinement, particularly in the spectral distribution at the polar location, $\psi_n = 30^\circ$. This is the location at which the jet noise is a maximum; and thus, the estimated shielding is most sensitive to the source noise. Work on this model will be continued.

The modified source formulation has been included in the jet shielding model. The model estimates not only the resultant jet shielding, but also the individual shielded and unshielded spectra. As in the development of the source model, differences are noted in the spectral distributions at the polar location, $\psi_n = 30^\circ$. These differences are expected to be resolved by the spectral amplitude function refinement. The discrepancies noted are not expected to affect the twin jet shielding estimate.

The twin jet shielding estimate is found to compare favorably with the measured data in the near downstream region where transmission dominates. Further downstream, the model overestimates the diffraction around the jet. This result is consistent with the point source shielding results, where jet widening increases the barrier effect of the shielding jet.

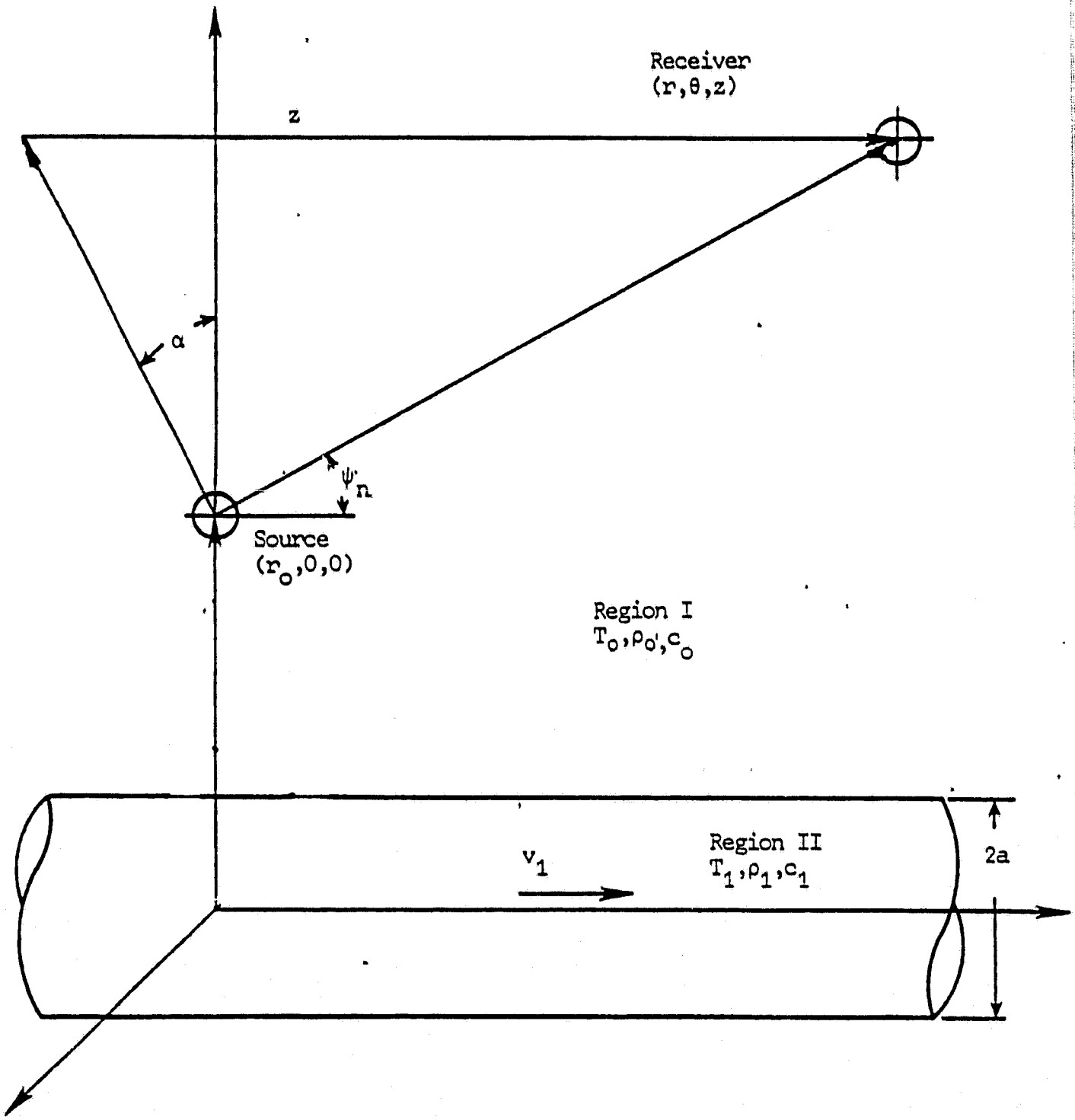

Figure 1. Schematic Representation of Point Noise Source Shielding Model.

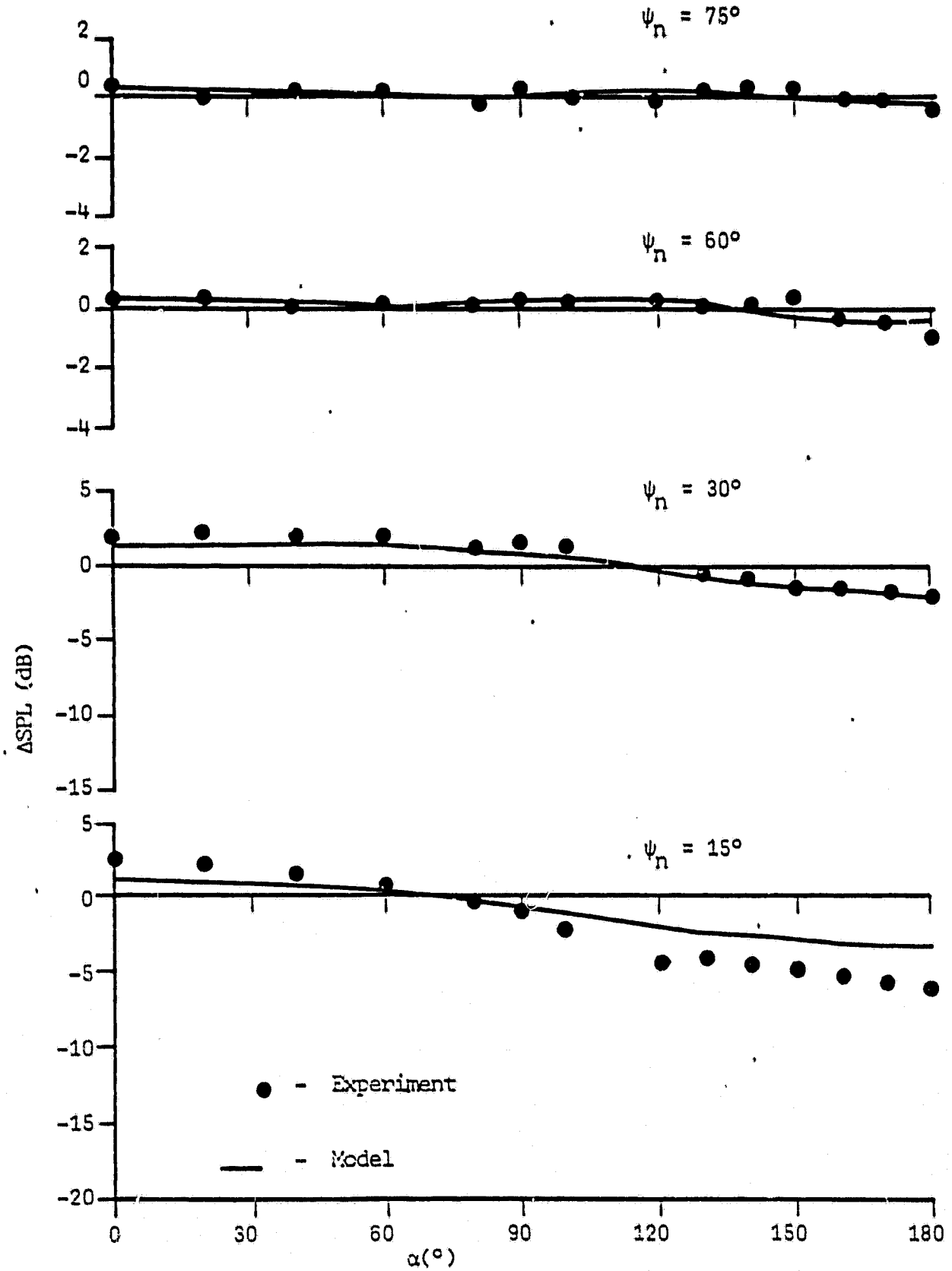

Figure 2. Azimuthal Directivity, Air jet, M=0.53, $k_o a$=0.56.

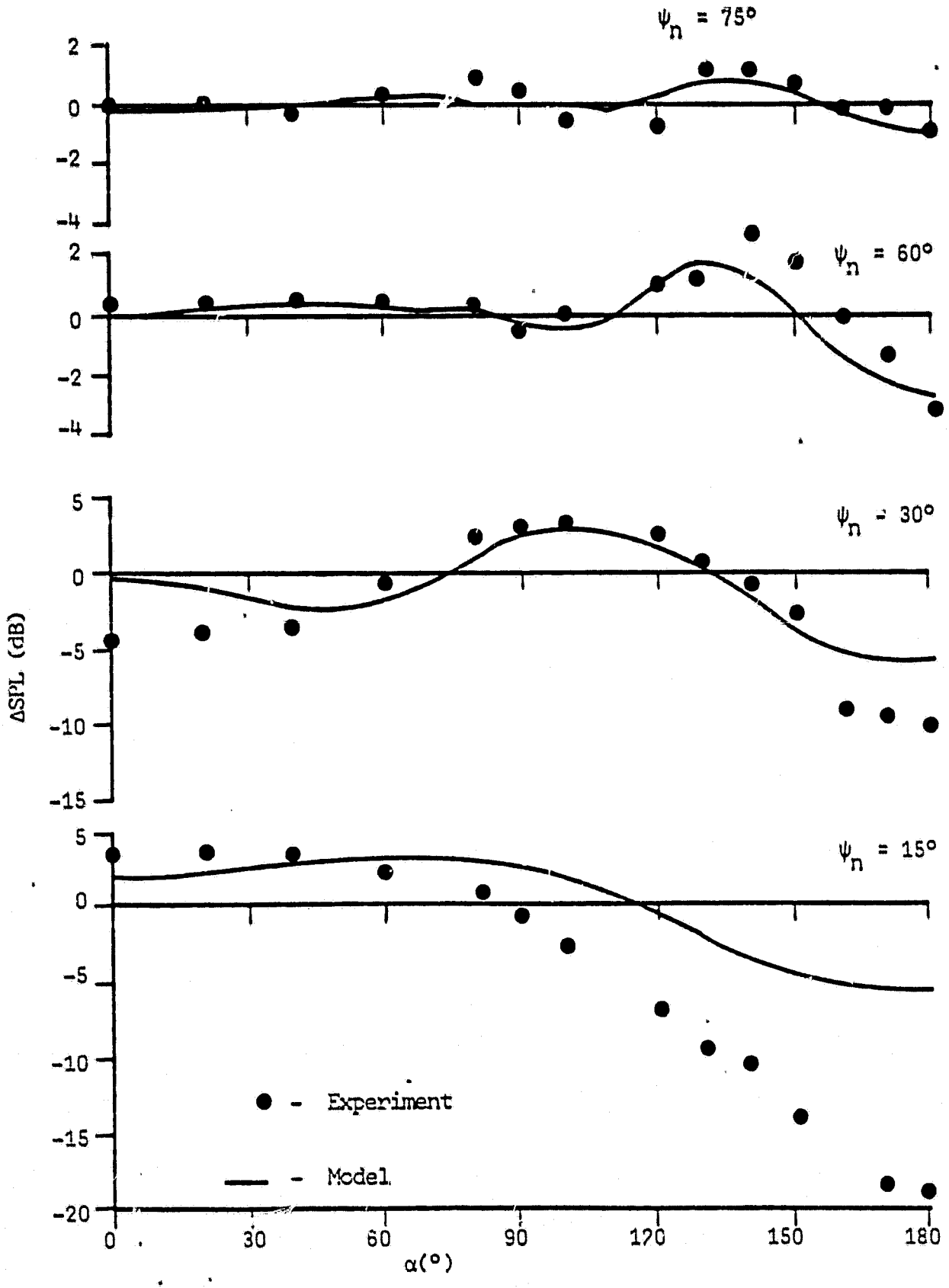

Figure 3. Azimuthal Directivity, Air jet, M=0.53, $k_o a$=1.60.

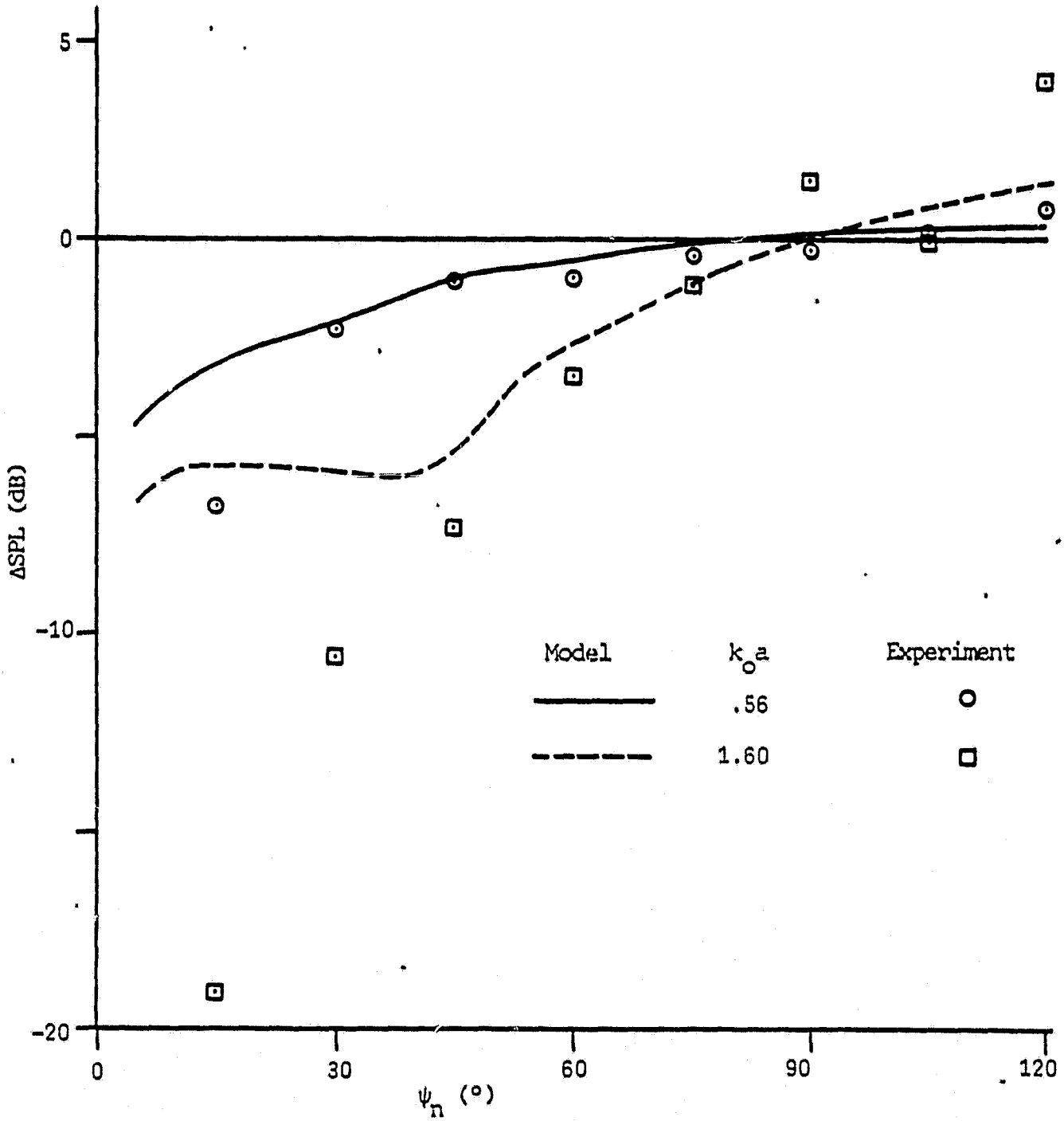

Figure 4. Polar Directivity, Air jet, M= 0.53, α = 180°

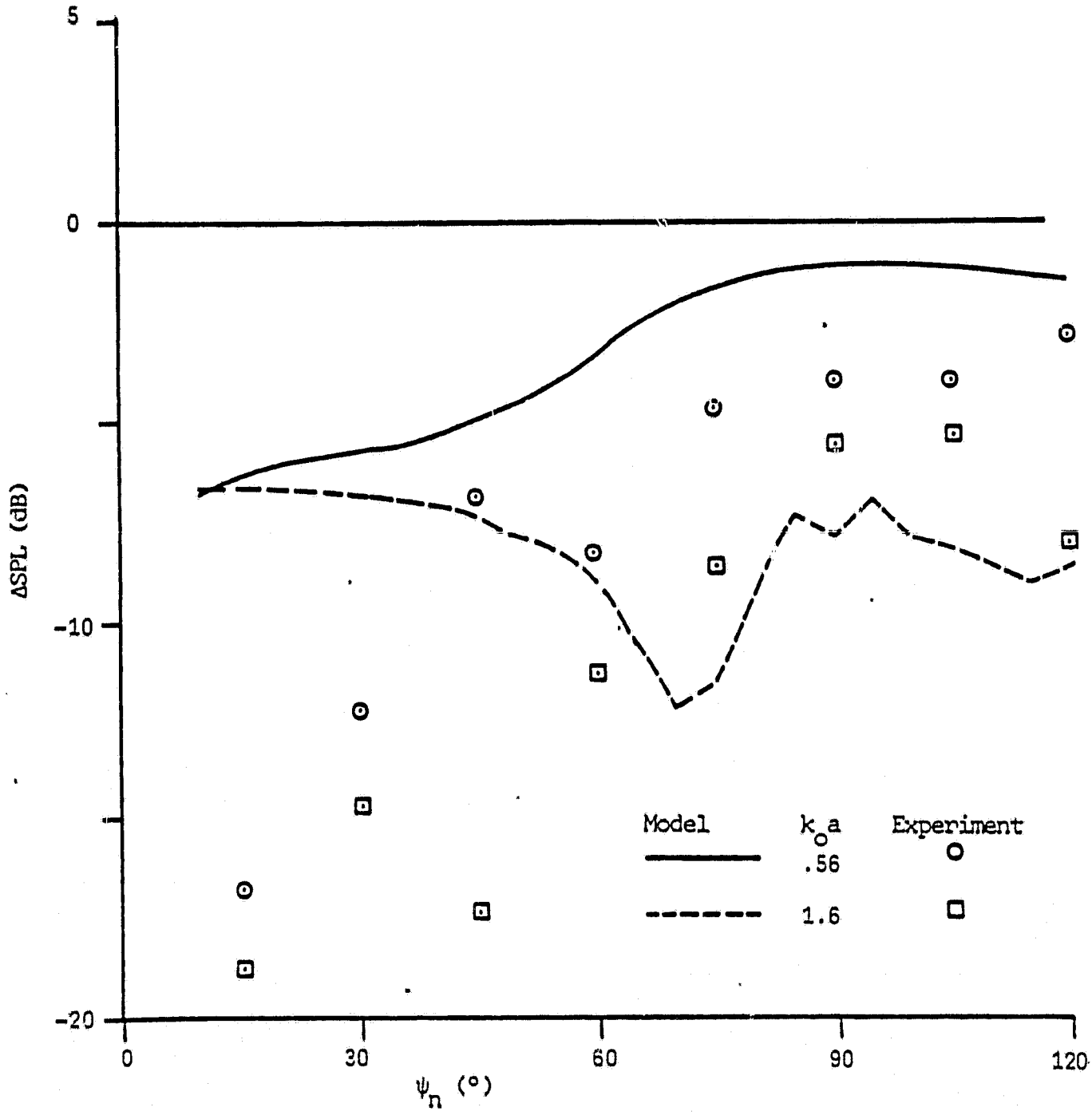

Figure 5. Polar Directivity, Helium Jet, M= 0.18, α = 180°

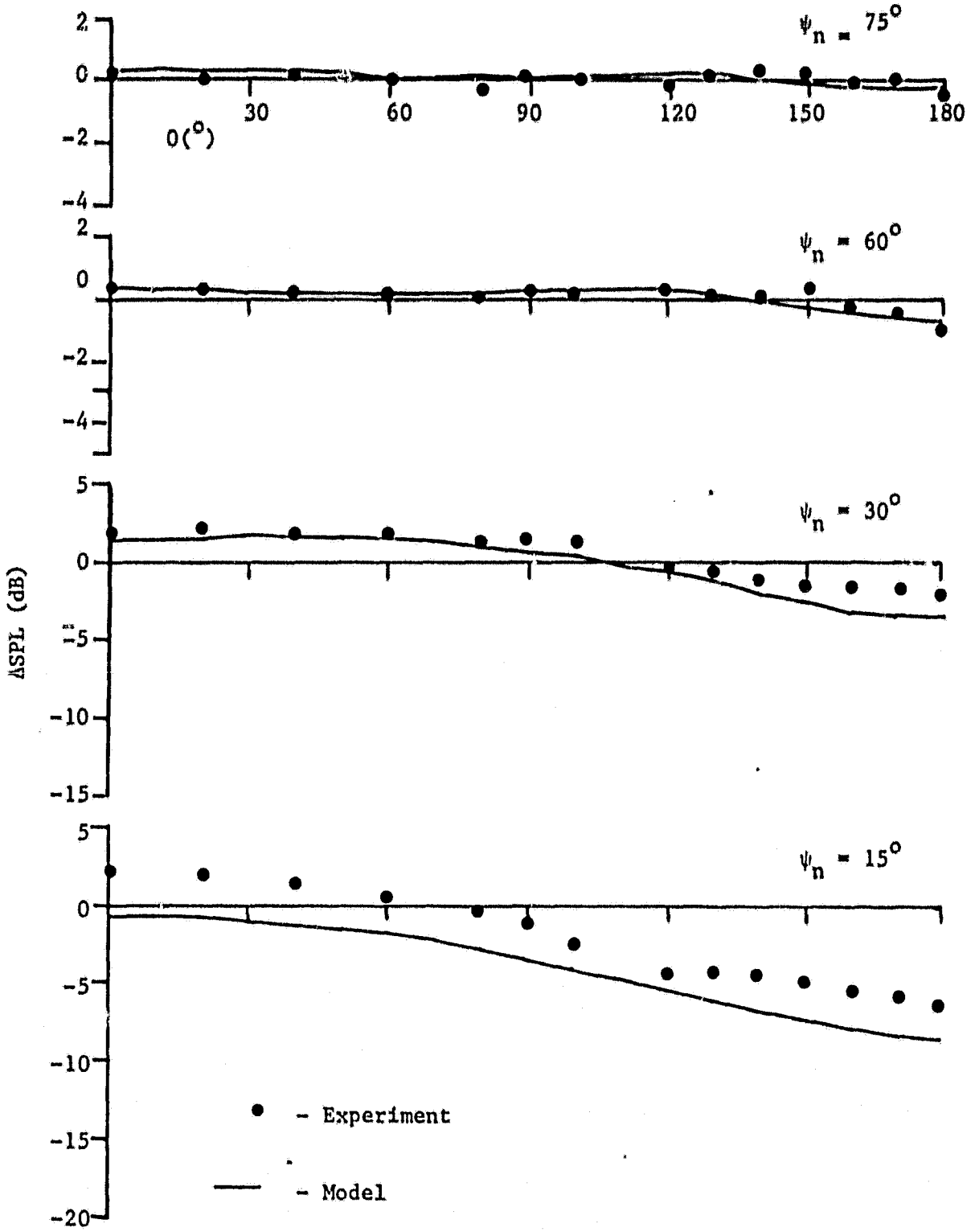

Figure 6. Azimuthal Directivity Function - Model with Shielding Jet Widening - $k_o a = 0.56$.

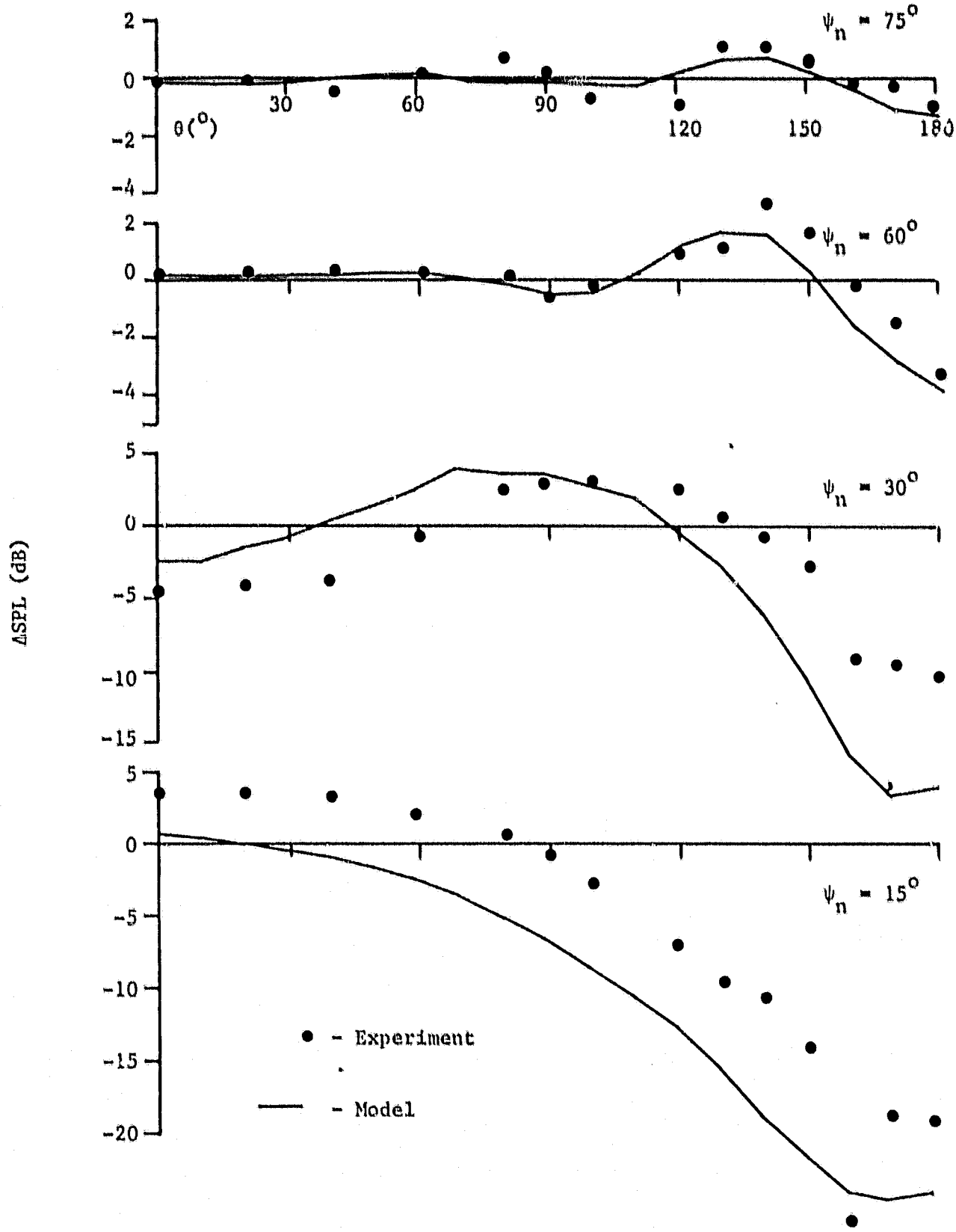

Figure 7. Azimuthal Directivity Function - Model with Shielding Jet Widening - $k_o a = 1.6$.

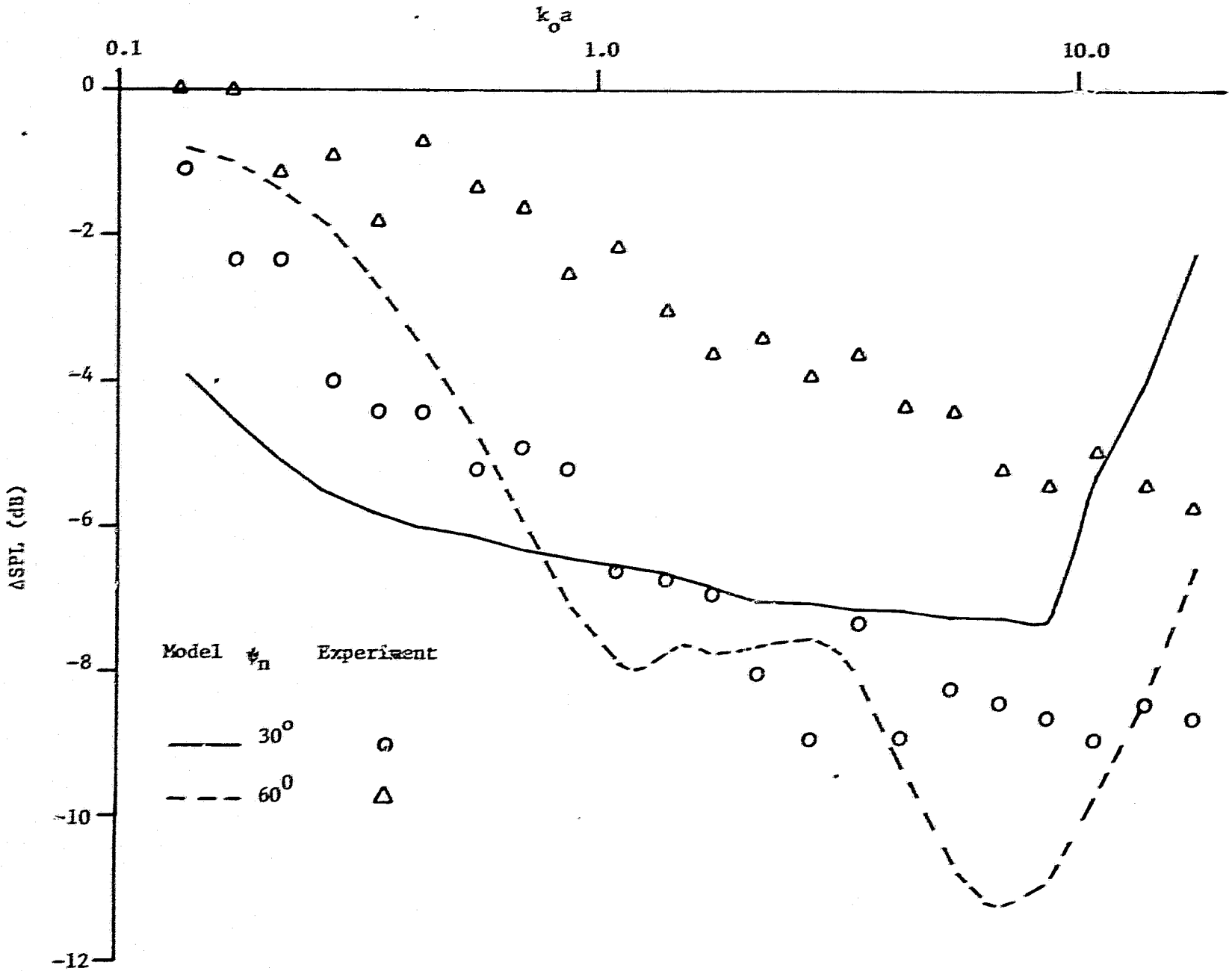

Figure 8. Twin Jet Shidleing Comparison with Point Noise Source - Heated Jet, $\alpha = 180^o$

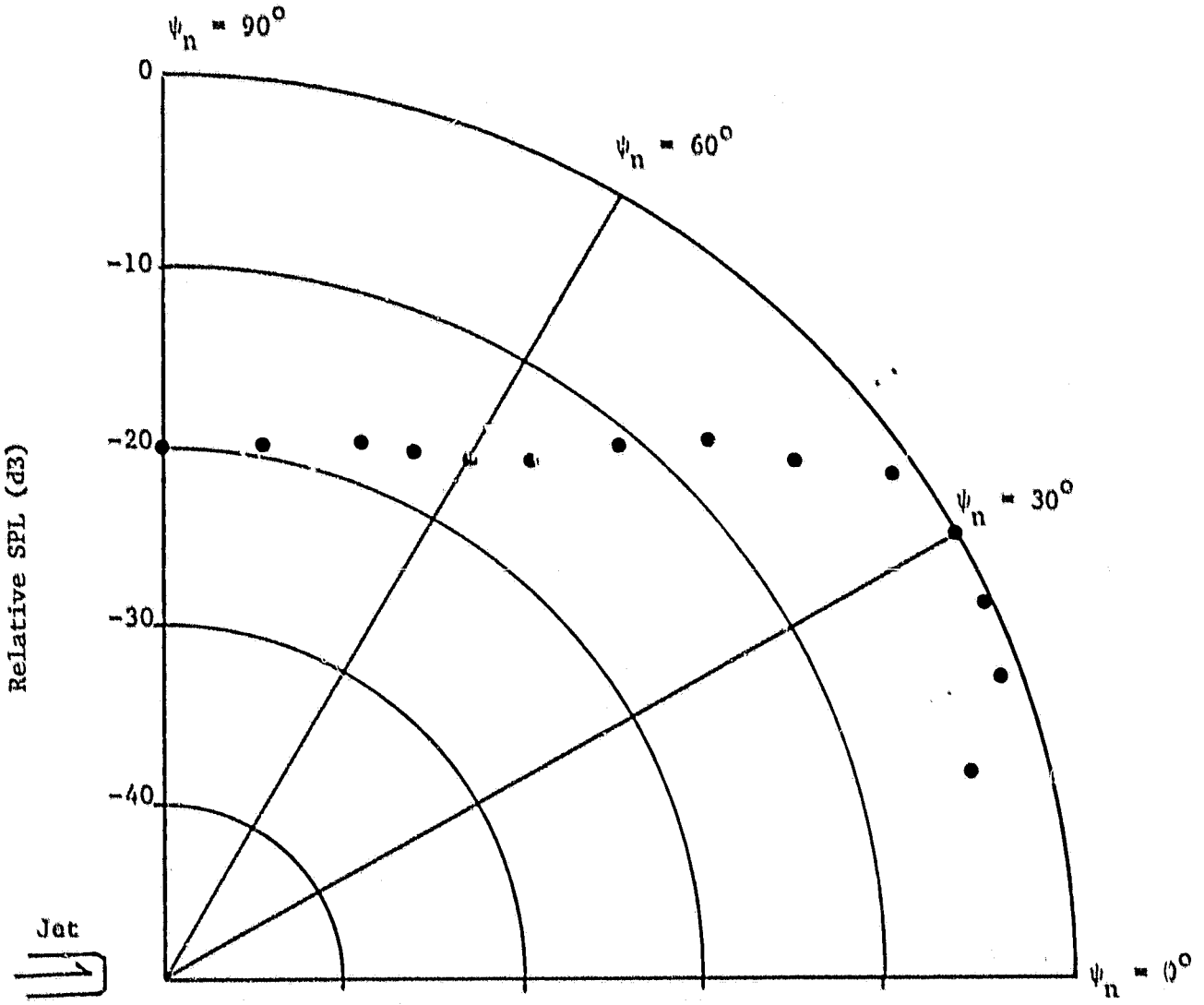

Figure 9. Typical Polar Directivity Plot of Unheated, Supersonic Jet.

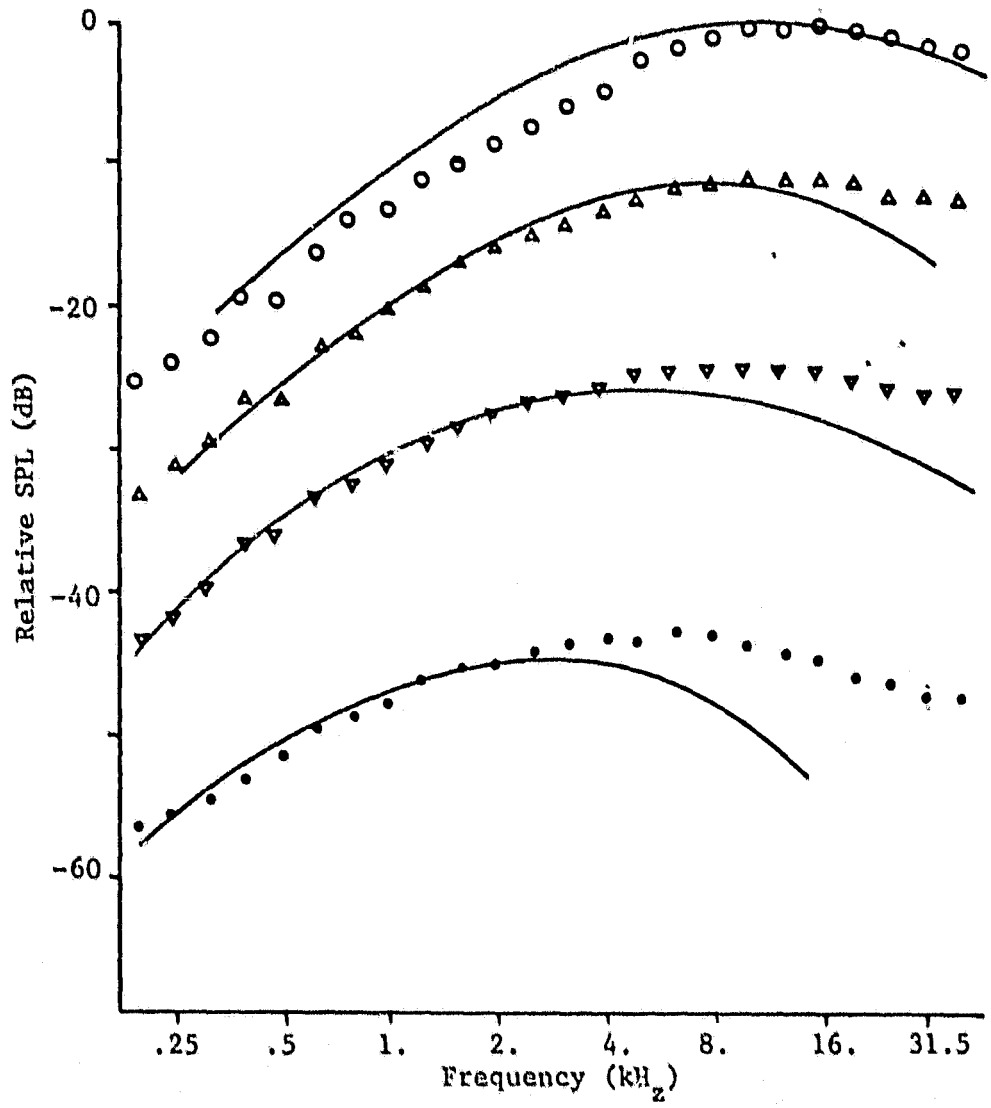

Figure 10. Relative Spectral Distribution of Isothermal Jet Noise at $\psi_n = 90^o$.

○ - v_j/c_o = 1.95, △ - U_j/c_o = 1.33, ▽ - U_j/c_o = 0.90

● - U_j/c_o = 0.50, solid lines - estimate

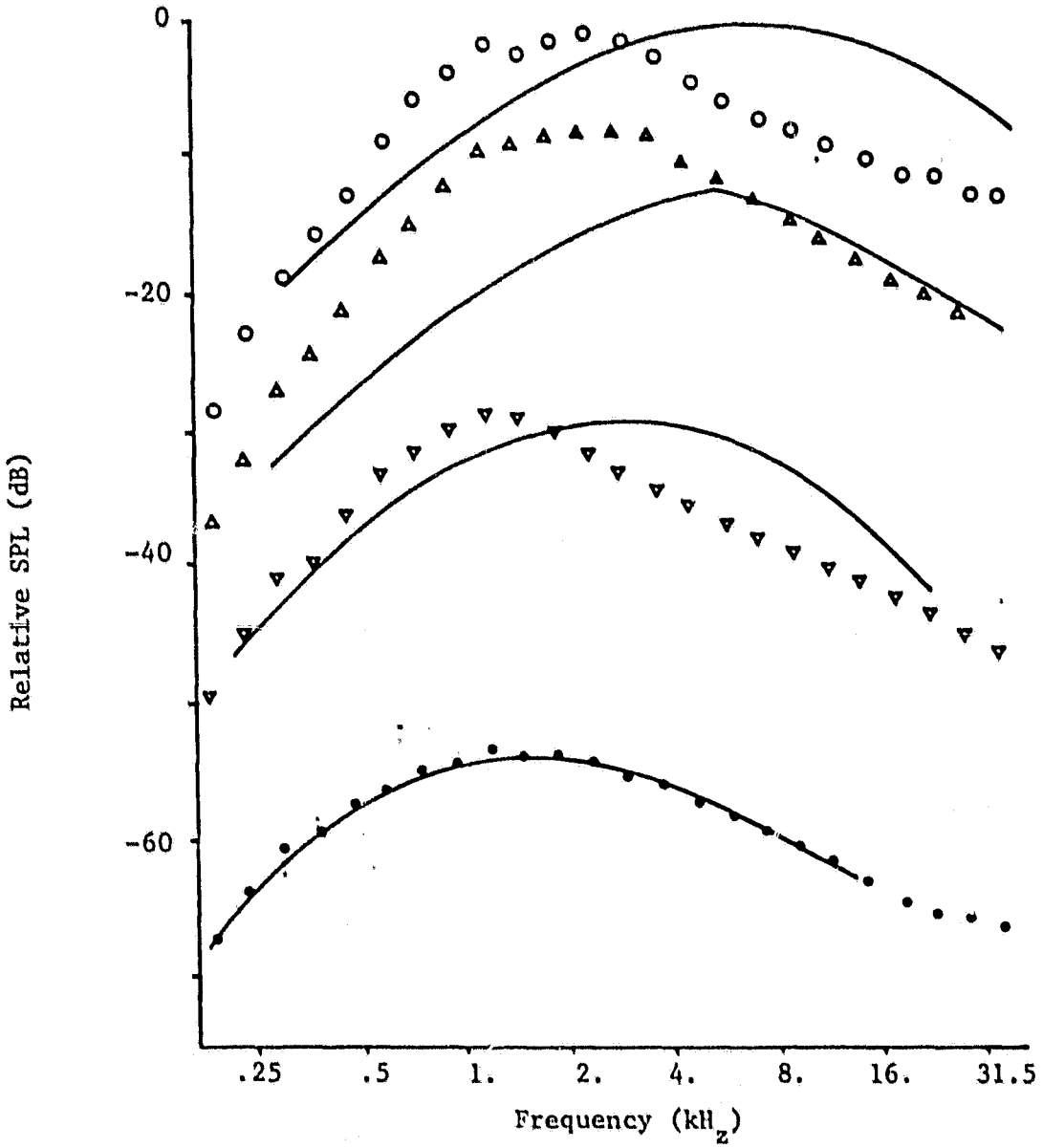

Figure 11. Relative Spectral Distribution of Isothermal Jet Noise at $\psi_n = 30^o$

○ - $U_j/c_o = 1.95$, Δ - $U_j/c_o = 1.33$, ∇ - $U_j/c_o = 0.90$

● - $U_j/c_o = 0.50$, solid lines - estimate

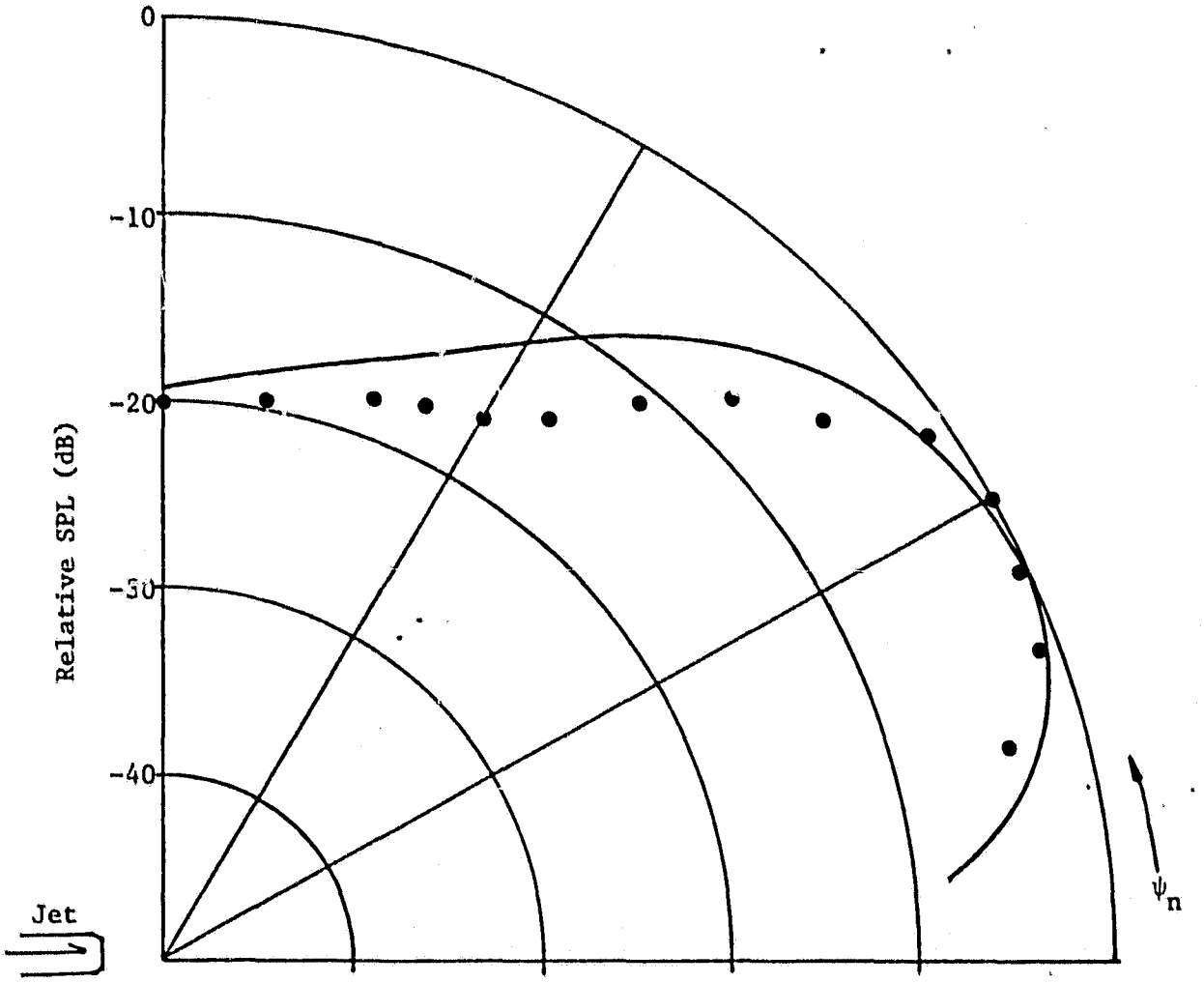

Figure 12. Polar Directivity of Unheated, Supersonic Jet Noise at St = 0.12.

● - measured,

—— - estimate

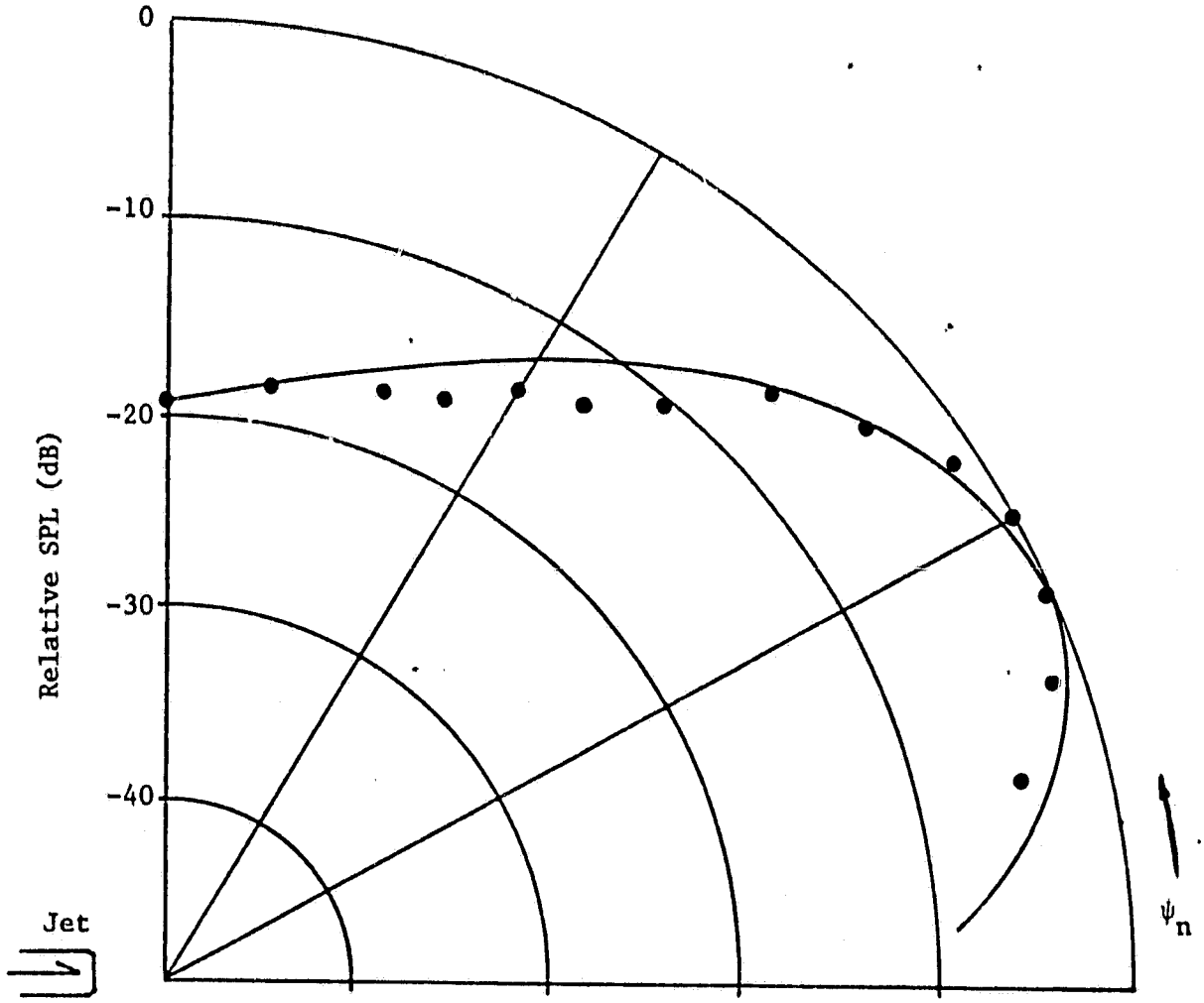

Figure 13. Polar Directivity of Unheated, Supersonic Jet Noise at St = 0.25

● - measured

—— - estimate

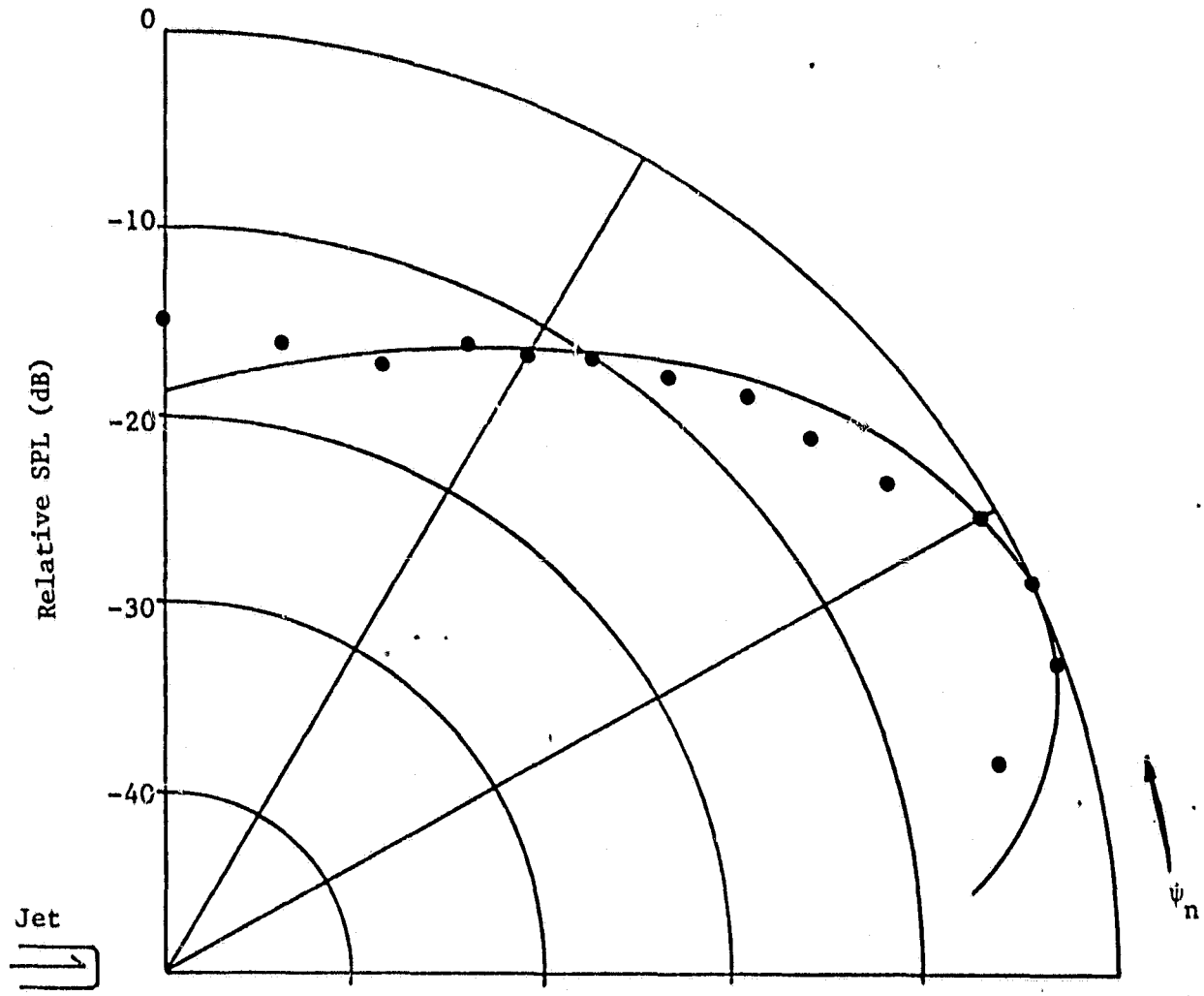

Figure 14. Polar Directivity of Unheated, Supersonic Jet Noise at St = 0.50.

● - measured

—— - estimate

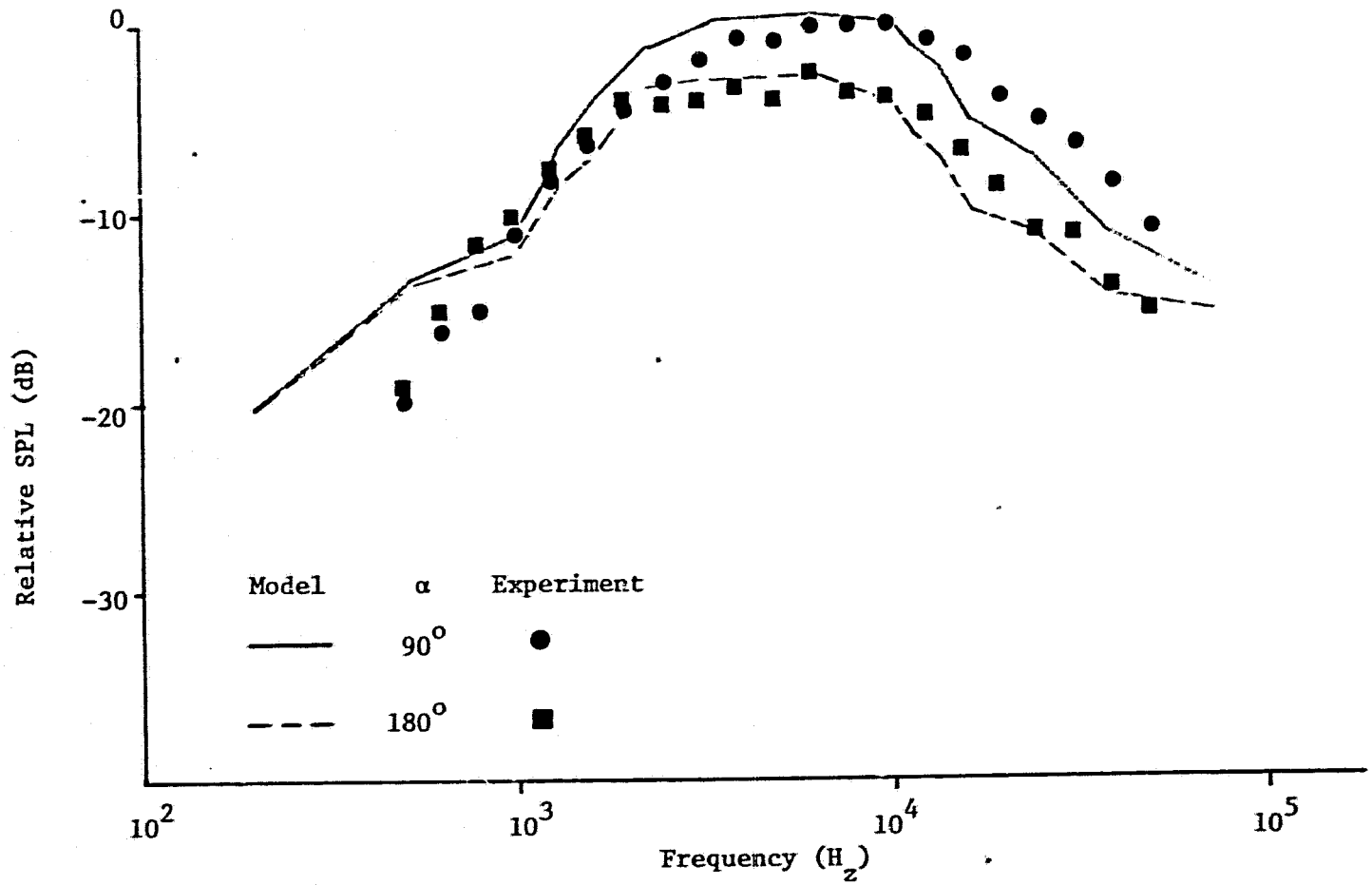

Figure 15. Spectral Distribution of Twin, Heated Jets, Comparing Unshielded ($\alpha = 90^o$) to shielded ($\alpha = 180^o$) Spectra. $\psi_n = 60^o$.

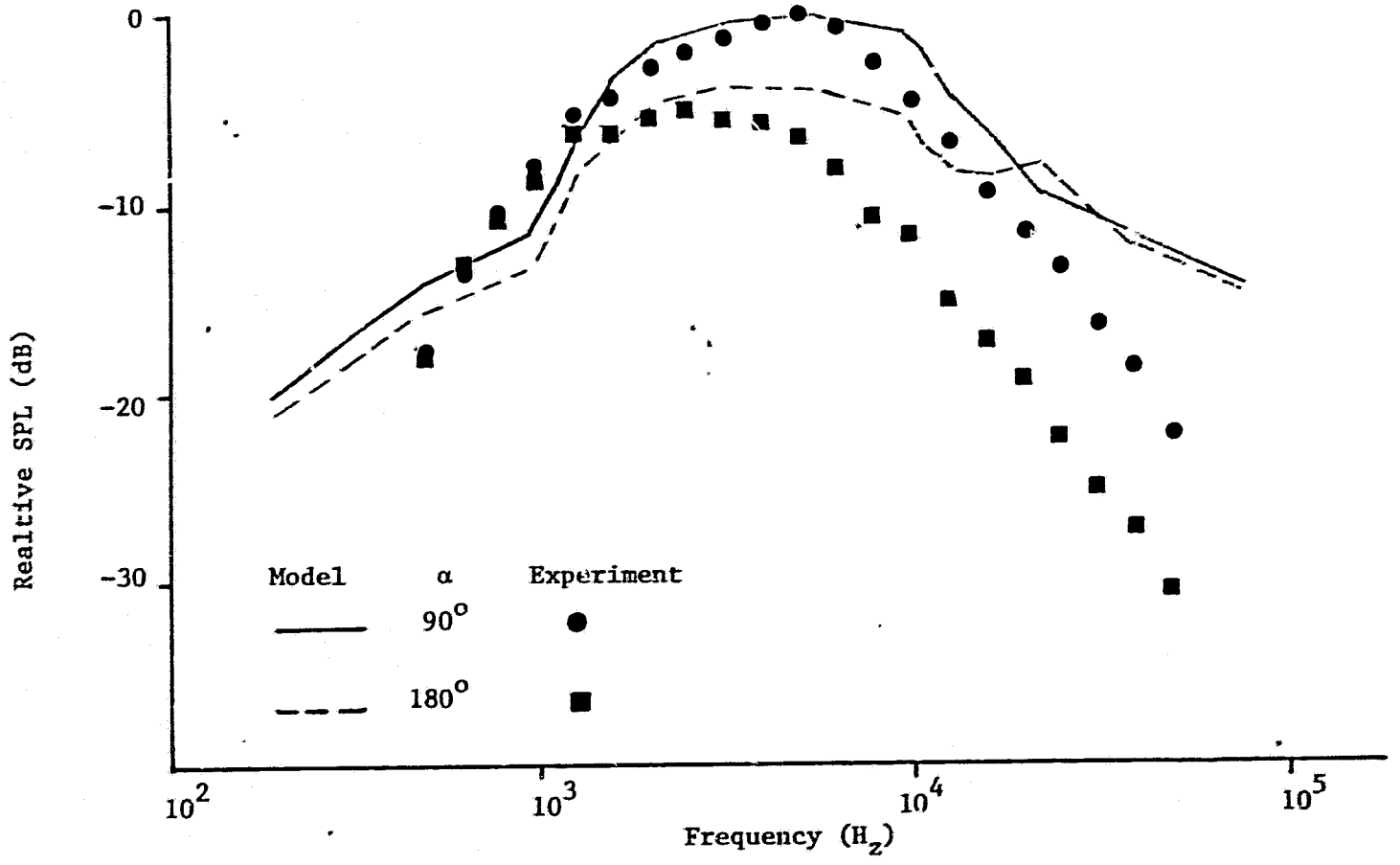

Figure 16. Spectral Distribution of Twin, Heated Jets; Comparing Unshielded ($\alpha = 90^o$) to Shielded ($\alpha = 180^o$) Spectra. $\psi_n = 30^o$.

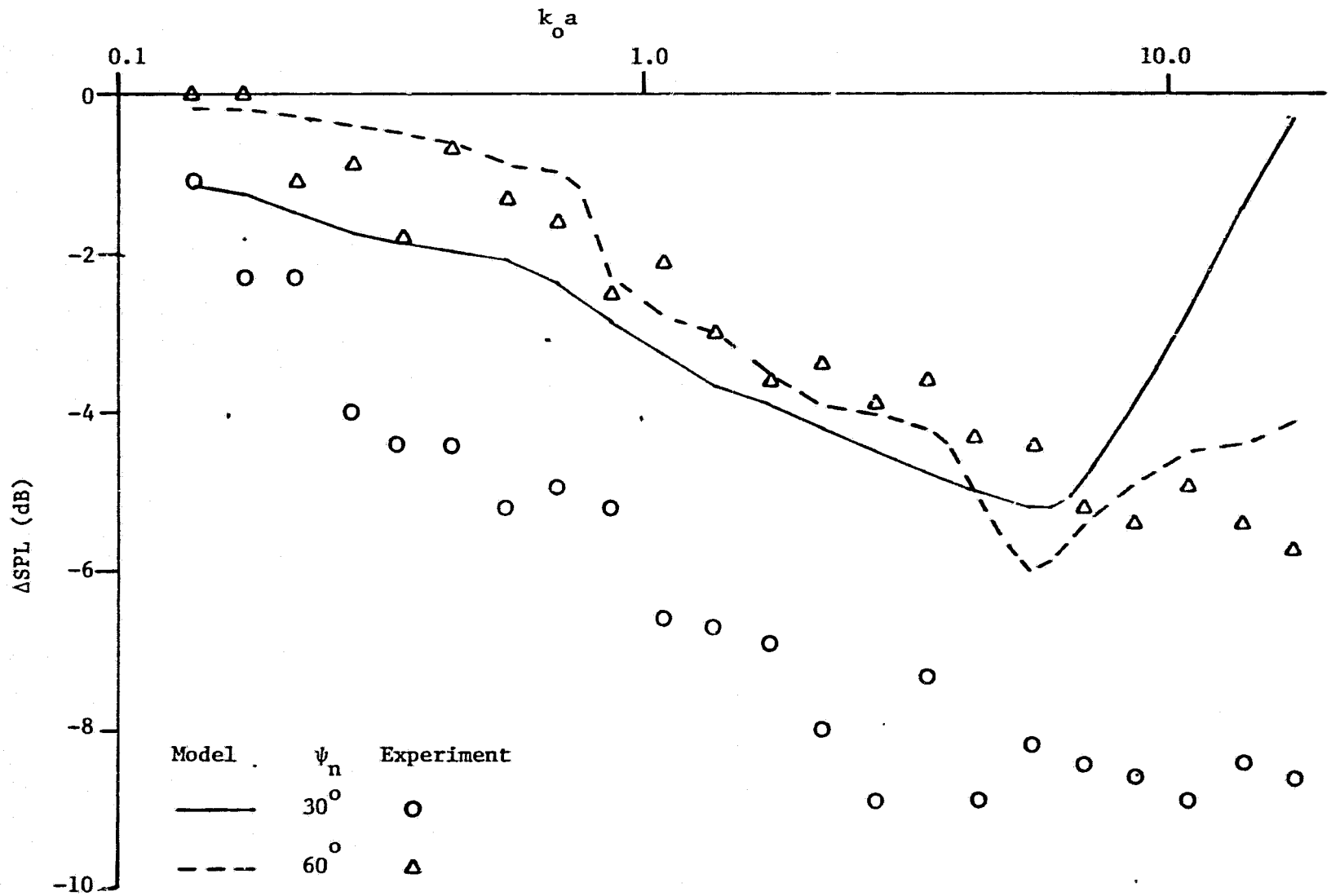

Figure 17. Twin Jet Shielding Comparison with Modefied Point Noise Source - Heated Jet, $\alpha = 180^\circ$

REFERENCES

1. Gerhold, C.H., "Analytical Study of Twin-Jet Shielding - Final Report" Report for NASA Grant # NAG-1-11. December 31, 1980.
2. Yu, J.C. and Fratello, D.J., Measurement of Acoustic Shielding by a Turbulent Jet, AIAA paper no. 81-2019. Presented at the AIAA 7th Aeroacoustics Conference, Oct. 5-7, 1981, Palo Alto, CA.
3. Yeh, C., "A Further Note on the Reflection and Transmission of Sound Waves by a Moving Fluid Layer", JASA, vol. 43, no. 6, p. 1454.
4. Kantola, R.A., "Shielding Aspects of Heated Twin Jet Noise." AIAA 4th Aeroacoustics Conference. Atlanta, GA., Oct.3-5, 1977.
5. Kim, Changho. Masters Thesis to be published, April 1982.
6. Yu, J.C. and Dosanjh, D.S., "Noise Field of Coaxial Interfacing Supersonic Jet Flaws", AIAA paper no. 71-152, 1971.
7. Ribner, H.S. The Generation of Sound by Turbulent Jets. Advances in Applied Mechanics, vol. VIII, pp. 103-182, 1964, Academic Press, New York, N.Y.
8. N.S.M. Nosseir, H.S. ribner, "Tests of a Theoretical Model of Subsonic Jet Noise", AIAA paper 75-436, Mar. 1975.
9. H.K. Tanna, P.D. Dean, "An Experimental Study of Shock-Free Supersonic Jet Noise", AIAA paper 75-480, Mar., 1975.